Downstream and upstream influence in river meandering. Part 1. General theory and application to overdeepening

By G. ZOLEZZI† AND G. SEMINARA

Dipartimento di Ingegneria Ambientale, Università di Genova, Via Montallegro 1, 16122, Genoa, Italy

Perturbations of channel geometry (like variations of channel curvature or channel width) in meandering rivers give rise to morphodynamic effects which display themselves through the development of large-scale perturbations of bottom topography in the form of stationary bars developing in the longitudinal direction. The latter may then drive the lateral migration of the channel by enhancing bank erosion at bar pools: through this mechanism local perturbations of channel geometry may affect the planimetric development of meandering rivers on large timescales. The problem tackled herein is whether such morphodynamic influence is invariably felt downstream as the commonly employed model of river meandering would suggest.

In order to solve this problem, we derive the exact solution of the linearized form of the mathematical problem of river morphodynamics. Linear analysis had pointed out the existence of a resonance phenomenon: in a linear (hence ideal) context, resonance occurs when the meander wavenumber and the width ratio of the channel take values (λ_R and β_R, respectively) such as to force free spatial modes of the system consisting of free bars which neither grow nor decay either in time or in space. Channels characterized by values of the width ratio β larger (smaller) than β_R are called super- (sub-)resonant. The present solution, which applies to channels with constant width and arbitrary curvature distribution, shows that two distinct scenarios may occur: downstream influence is associated with sub-resonant channels and vice versa dominant upstream influence occurs in super-resonant channels. Small-amplitude waves of bottom topography are shown to migrate downstream in the former case and may migrate upstream in the latter, as resonance also defines the threshold conditions below (above) which small-amplitude alternate bar perturbations (may) migrate downstream (upstream).

These results have several implications. In the present paper we examine the overdeepening phenomenon whereby abrupt variations of channel curvature, as in sequences of straight and constant curvature reaches, lead to sequences of stationary alternate bars with amplitude decaying in the longitudinal direction. We show that, along with downstream overdeepening, an upstream overdeepening scenario is predicted in the super-resonant regime.

Implications of the upstream influence on planimetric development of meandering rivers are investigated in Part 2.

---

† Present address: Dipartimento di Ingegneria Civile e Ambientale, Università di Trento, Via Mesiano 77, 38050, Trento, Italy.

1. Introduction

Rivers are self-formed features which develop as a result of bed and bank erodibility. The ability to predict such development is then strictly dependent on the capability of modelling flow field, bottom topography and bank erosion conveniently.

A number of models have been proposed in the recent past for meandering rivers. Among them the model of Ikeda, Parker & Sawai (1981), more recently corrected by Johannesson & Parker (1989), is the most popular and will hereinafter be referred to as the standard model. Most numerical simulations of the planimetric evolution of meandering rivers published since 1984 have been based on the use of the above model (Beck 1984; Beck, Melfi & Yalamanchili 1984; Parker & Andrews 1986; Furbish 1988; Howard 1996; Sun *et al.* 1996; Stolum 1996). Crosato (1990) employed a numerical model based on the solution of the full De St Venant equations.

In the context of the standard model, the local value of the rate of lateral channel shift at some specified cross-section is determined by the perturbation of the flow-field bottom topography evaluated at the banks and is found to consist of two contributions:

  (i) the first is proportional to some measure of the local curvature of the channel axis;

  (ii) the second accounts for the effect of the spatial distribution of channel curvature upstream of the given cross-section.

In the context of the standard model, the morphodynamic influence invariably acts in the downstream direction. Let us think of the following simple channel configuration: a curved reach with constant curvature of the channel axis connected to two straight reaches located upstream and downstream the curved reach, respectively. Under such conditions, the standard model predicts that the presence of the curved reach is invariably felt morphodynamically only in the curved reach itself and in the straight reach located downstream. This is in agreement with the observations of Struiksma *et al.* (1985), who showed that at the entrance region of a curved reach, bottom topography adjusts to the new equilibrium, asymptotically characterized by a longitudinally uniform transverse bed profile, through a sequence of damped steady oscillations of transverse bed slope occurring downstream of the abrupt change of channel curvature. The development of such non-migrating spatially decaying bars at the bend entrance represents the clearest example of downstream influence in river morphodynamics. This phenomenon, called overdeepening, was explained theoretically by Struiksma *et al.* (1985) and later confirmed by Johannesson & Parker (1989).

Yet, a natural question arises: are there any conditions such that the morphodynamics of meandering rivers is characterized by upstream influence? In the particular case of the overdeepening phenomenon the above question can be rephrased by asking whether upstream overdeepening ever occurs.

The type of influence we are discussing here does not arise in the context of one-dimensional modelling of river morphodynamics. The critical conditions correspond to the unit Froude number, which acts as the crucial parameter; it is well known, since the work of de Vries (1969), that an upstream influence may indeed occur in supercritical streams on the slow timescale associated with bottom evolution.

We are concerned here with two-dimensional steady perturbations of bottom topography.

Revisiting the analysis of river meandering, we show that the picture arising from the classical findings based on the standard model is not complete. In fact, the exact

solution of the linearized problem of river meandering shows that two scenarios may occur. For channels characterized by width to depth ratios (2β) smaller than a threshold value ($2\beta_R$), downstream influence dominates the morphodynamics and the picture is qualitatively similar to that arising from the standard model. On the contrary, if β exceeds β_R, upstream influence dominates the morphodynamics, and the picture is drastically different from that arising from the standard model.

The value of β_R coincides with the resonant value of Blondeaux & Seminara (1985), hence, upstream influence is associated with super-resonant conditions whereas downstream influence occurs in sub-resonant channels. The occurrence of upstream influence is strictly associated with the ability of sufficiently long two-dimensional bottom perturbations of the alternate bar type to migrate upstream (see § 7).

These results are based on a linearized treatment of flow and bed topography in meandering channels. We are aware of its validity limits. However, the importance of such an approach arises from its relative simplicity which makes it amenable to an analytical treatment allowing us to disclose some basic mechanisms operating in river morphodynamics. Such mechanisms may then be quantitatively evaluated in a more refined way with the help of numerical solutions of the full nonlinear problem.

In this paper we derive a two-dimensional formulation of the mathematical problem governing flow and bed topography in erodible channels with an arbitrary distribution of curvature of the channel axis. Such derivation involves some novel features as it accounts for the dispersive transport of momentum by the secondary flow calculated through the approach of Seminara & Solari (1998) which is not restricted to the case of small perturbations of flow and bed topography. We then derive the exact general solution of the linearized form of the above differential problem and discuss the implications of such solutions as regards the problem of upstream and downstream influence in river morphodynamics.

An application of the linear solution is then proposed to the problem of overdeepening. Comparison with the experimental observations of Struiksma *et al.* (1985) is performed and shows that the phenomenon of downstream overdeepening is correctly reproduced by the present model. The conditions for the occurrence of upstream overdeepening are also examined and exemplified, while preliminary experimental observations (Guala *et al.* 1999) are strongly suggestive of the actual occurrence of such a phenomenon.

In Part 2 (Seminara *et al.* 2001) the solution derived here is set as the basis of a model of planimetric evolution of meandering rivers.

2. Formulation of a three-dimensional model

The starting point for the derivation of a two-dimensional model of river morphodynamics is an appropriate three-dimensional form of the continuity and momentum equation for the fluid phase, which must be coupled to an evolution equation for bed topography. Reynolds equations for the fluid phase and a two-dimensional version of the Exner equation for the solid phase along with appropriate dynamic equations for the solid phase accounting for effects associated with a sloping topography fit our needs.

Let us then consider a meandering river characterized by a cohesionless bed and constant width $2B^*$ (figure 1). The latter assumption may be readily relaxed but is maintained here in order to keep the algebraic work at the lowest level of complexity. We refer the flow field and bed topography to an orthogonal reference system (s^*, n^*, z^*) where s^* is the longitudinal coordinate of the channel axis assumed to lie on
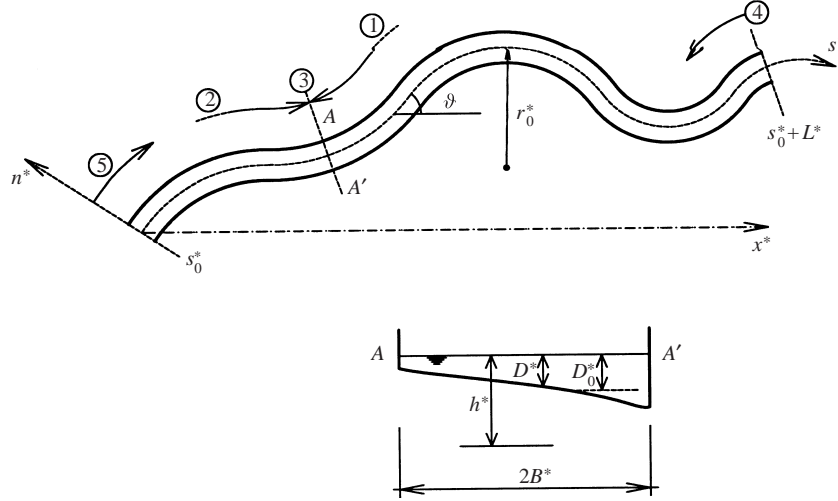
FIGURE 1. Sketch of a meandering channel and notation. The regions of influence of the five different contributions in the exact solution (6.6) are also indicated.

a plane, n^* is the transverse coordinate defined along a horizontal axis orthogonal to s^*, and z^* is the coordinate of the axis orthogonal to s^* and n^* and pointing upwards.

Notice that hereinafter an asterisk denotes a dimensional quantity. Let $\mathscr{C}^*(s^*) = r_0^{*-1}$ be the distribution of curvature of the channel axis. Moreover, we denote by (u^*, v^*, w^*) the mean velocity vector (averaged over turbulence) in the same reference frame, by $h^*(s^*, n^*)$ the local value of the free-surface elevation relative to some horizontal datum, and by $D^*(s^*, n^*)$ the local value of the flow depth.

It is convenient to make the above quantities dimensionless as follows:

$$(s^*, n^*) = B^*(s, n), \qquad z^* = D_0^* z, \qquad (2.1a, b)$$

$$(h^*, D^*) = D_0^*(h, D), \quad (u^*, v^*, w^*) = U_0^*(u, v, w), \qquad (2.1c, d)$$

having denoted by D_0^* and U_0^* some typical flow depth and average speed. The simplest choices for D_0^* and U_0^* are the values of flow depth and average cross-sectional speed of a uniform flow characterized by the same value of flow discharge and channel width as for the meandering river considered herein and channel slope equal to the average slope of the meandering reach.

We may then write Reynolds equations in dimensionless form in terms of the above coordinate system to find:

$$N(u^2)_{,s} + (uv)_{,n} + \beta(uw)_{,z} + 2v_0 N\mathscr{C}uv = -N\left(\frac{1}{F_0^2}h_{,s} - \beta C_{f0}\right) + \beta\sqrt{C_{f0}}(v_T u_{,z})_{,z},$$

$$(2.2)$$

$$N(uv)_{,s} + (v^2)_{,n} + \beta(vw)_{,z} + v_0 N\mathscr{C}(v^2 - u^2) = -\frac{1}{F_0^2}h_{,n} + \beta\sqrt{C_{f0}}(v_T v_{,z})_{,z}, \qquad (2.3)$$

$$Nu_{,s} + \left(\frac{\partial}{\partial n} + v_0 N\mathscr{C}\right)v + \beta w_{,z} = 0, \qquad (2.4)$$

where N^{-1} is the longitudinal metric coefficient of the coordinate system, β is the half width to depth ratio, F_0 and C_{f0} are the Froude number and friction coefficient

of the reference uniform flow and v_T is a dimensionless eddy viscosity. The above parameters read:

$$\beta = \frac{B^*}{D_0^*}, \quad v_0 = \frac{B^*}{R_0^*}, \quad F_0 = \frac{U_0^*}{\sqrt{g D_0^*}}, \tag{2.5a–c}$$

$$v_T = \frac{v_T^*}{\sqrt{C_{f0}} U_0^* D_0^*}, \quad N = [1 + v_0 n \mathscr{C}(s)]^{-1}, \tag{2.5d, e}$$

having denoted by R_0^* a typical value of channel curvature, say its minimum value in the meandering reach.

Notice that in (2.2)–(2.4) we have already incorporated the hydrostatic distribution of mean pressure predicted by the z-component of Reynolds equations for shallow motions i.e. motions characterized by longitudinal and lateral scales much larger than a typical flow depth. Furthermore in (2.2)–(2.3) we have neglected normal Reynolds stresses and the tangential stress T_{sn}. The latter assumption is again justified by the assumed slowly varying character of the flow field. In fact, river cross-sections are typically fairly wide, and meandering occurs typically on spatial scales of the order of several channel widths. Hence, the slowly varying assumption appears to be reasonable, although it may possibly fail within the side boundary layers when the banks are steep and close to sharp fronts of the type associated with bar migration. We will assume that the side boundary layers play a passive role and exclude them from our analysis of the flow field which will be restricted to the central region of the flow. Again, we deliberately ignore the possible coexistence of free migrating and forced steady bars of the type observed by Whiting & Dietrich (1993) in large-amplitude meanders which is still an unsettled question (but see Tubino & Seminara 1990). However, it is a fact that the typical shape of meanders can be predicted by ignoring the possible presence of migrating features (Parker, Diplas & Akiyama 1983). This suggests that the latter are likely to enhance the process of bank erosion driven by forced features (maybe triggering the process when migrating and forced features are in phase with each other) but they do not alter the essential characteristics of meander development which occurs, anyway, on timescales which largely exceed the timescale associated with free bar migration.

The boundary conditions to be associated with (2.2)–(2.4) require:
no slip at the bottom, hence

$$u = v = w = 0 \qquad (z = h - D + z_0), \tag{2.6}$$

with z_0 dimensionless conventional reference elevation taken to coincide with local conditions;
stress continuity at the free surface, hence

$$u_{,z} = v_{,z} = 0 \qquad (z = h), \tag{2.7}$$

where the free surface has been approximately taken to coincide with its tangent plane;
impermeable sidewalls.
Having ignored the sidewall boundary layers the latter condition is reinforced by requiring that the net flux exchanged between sidewall layers and the central region must vanish. Hence,

$$\int_{h-D+z_0}^{h} v \, \mathrm{d}z = 0, \tag{2.8}$$

The formulation of the three-dimensional problem is completed by the equations of sediment continuity along with a dynamic equation for sediment motion. Let $q \equiv (q_s, q_n)$ be the unit volumetric sediment discharge vector made dimensionless in the form

$$q = \frac{q^*}{\sqrt{(s-1)gd_s^{*3}}}, \tag{2.9}$$

where s is the relative density of the sediments, d_s^* is some typical grain size (say d_{50}^*) and g is acceleration due to gravity.

For uniform plane beds, we may write

$$q = q_0(\tau_*, R_p)\frac{t^*}{|t^*|}, \tag{2.10}$$

where t^* is the tangential component of the stress vector acting on the bed, R_p is the particle Reynolds number (defined as $\sqrt{(s-1)gd_s^{*3}}/\nu$) and τ_* is the Shields stress which reads:

$$\tau_* = \frac{|t^*|/\varrho}{(s-1)gd_s^*}. \tag{2.11}$$

Several proposals for the discharge predictor q_0 are available in the literature. In the following, we have employed two different predictors. The formula of Parker (1990) refers to bedload transport only and has the advantage of behaving smoothly as the Shields stress tends to zero. Notice that (2.10) predicts that the average direction of bedload transport coincides with the direction of the average bottom stress.

The simplest way to extend (2.10) to bed topography fields slowly varying in space is to assume that

$$q = q(\tau_*, R_p, \nabla_h \eta), \tag{2.12}$$

where $\nabla_h \equiv (\partial/\partial s, \partial/\partial n)$. Taking advantage of the assumption of slow spatial variations of flow and bed topography, we linearize (2.12) subject to the constraint that q must tend to the form (2.10) as $\nabla_h \eta$ tends to vanish. On purely dimensional grounds we then readily find:

$$q = q_0(\tau_*; R_p)\left[\frac{t^*}{|t^*|} + \mathbf{G} \cdot \nabla_h \eta\right], \tag{2.13}$$

where $\mathbf{G}$ is a 2×2 matrix which describes how gravity, acting on particles moving on a sloping surface, affects the direction and intensity of bedload motion, driving some deviation of the average particle trajectory from the direction of mean bottom stress.

It is known through both theoretical and experimental works (see in particular Sekine & Parker 1992; Kovacs & Parker 1994; Talmon, Struiksma & Van Mierlo 1995) that in a linearized context the diagonal elements of $\mathbf{G}$ may be assumed to vanish whereas $G_{\sigma\sigma}$ and $G_{\nu\nu}$ may be estimated in the form:

$$G_{\sigma\sigma} = -\frac{\tau_{*c}}{\mu q_0}\frac{\mathrm{d}q_0}{\mathrm{d}\tau_*}, \quad G_{\nu\nu} = -\frac{r}{\tau_*^m}, \tag{2.14}$$

where τ_{*c} is the critical value of Shields stress, μ is the dynamic friction coefficient and (σ, ν) is an orthogonal coordinate system such that the σ direction coincides with the direction of mean bottom stress. Various fairly equivalent suggestions have been made for the exponent m and the empirical coefficient r. We follow Talmon *et al.* (1995) and take $m = \frac{1}{2}$ with r in the range of 0.5–0.6 approximately.

We have also employed Engelund & Hansen's (1967) formula for q_0, concerning the total load. However, for the relatively small values of the Shields stress considered

below ($\tau_* \leqslant 0.3$), transport occurs dominantly as bedload for grain sizes as small as 0.2 mm. The use of Engelund & Hansen's (1967) approach allows us to account for the effects of bedforms on flow resistance.

The formulation of the problem of meander morphodynamics is then completed by the two-dimensional Exner equation which, under steady conditions and in the coordinate system (s, n), reads

$$\nabla_h \cdot \boldsymbol{q} = N q_{s,s} + \left(\frac{\partial}{\partial n} + v_0 N \mathscr{C} \right) q_n = 0 \, . \tag{2.15}$$

The boundary conditions to be associated with (2.15) are:

$$q_n|_{n=\pm 1} = 0, \tag{2.16}$$

along with the value of the total sediment discharge carried by the stream.

3. An extension of Kalkwijk & De Vriend (1980) flow decomposition and the general structure of secondary flow

It is well known, since the pioneering work of Rozovskij (1957), that, in constant-curvature channels, centrifugal effects lead to the establishment of a secondary flow with vanishing depth average. When curvature varies in the longitudinal direction, a second component of the secondary flow with non-vanishing depth average is induced by topographic and inertial effects. The nonlinear character of the governing equations implies an interaction between the two components of the secondary flow. Odgaard (1986) first attempted to analyse flow and bed topography in channels with spatially varying curvature; his approach involves a number of heuristic approximations which prevented his model from predicting the possibility of upstream influence, which is the subject of the present investigation.

We now wish to derive a depth-averaged form of the governing equations where the memory of the centrifugally induced secondary flow with zero average is preserved.

In order to achieve this goal, we extend the flow decomposition originally proposed by Kalkwijk & De Vriend (1980) for the fixed-bed case. Hence, we write

$$v = v_0 v_0(\zeta, n, s) + V(n, s) \mathscr{F}_0(\zeta), \tag{3.1}$$

$$h = v_0 h_0(n, s) + \hat{H}(n, s), \tag{3.2}$$

$$u = \mathscr{F}_0(\zeta) U(n, s). \tag{3.3}$$

In (3.1)–(3.3) ζ is the z-coordinate made dimensionless in the form:

$$\zeta = \frac{z - \eta(s, n)}{D(n, s)}, \tag{3.4}$$

and $\mathscr{F}_0(\zeta)$ is the velocity distribution of the uniform flow with local flow characteristics. Furthermore, $v_0(\zeta, s, n)$ is the local distribution of the centrifugally induced secondary flow, hence

$$\int_{\zeta_0}^1 v_0(\zeta, n, s) \, \mathrm{d}\zeta = 0, \tag{3.5}$$

where ζ_0 is equal to $\zeta(z_0; s, n)$.

In order to be able to employ (3.1)–(3.3) as the starting point for the derivation of two-dimensional governing equations for U, V and $\hat{H}$, we must determine the form of v_0 and h_0 appropriate to channels with arbitrary distribution of curvature

of the channel axis. An appropriate extension of Seminara & Solari's (1998) analysis referring to constant-curvature channels will fulfil our aim.

Equation (2.3), rewritten in terms of the coordinate system (ζ, s, n), becomes:

$$\beta\sqrt{C_{f0}}[\mathcal{N}(\zeta)v_{,\zeta}]_{,\zeta} = D\mathcal{F}_0 v_{,s} + \mathcal{F}_0 v_{,\zeta}[(1-\zeta)D_{,s} - h_{,s}] - v_0 \mathcal{C} D U \mathcal{F}_0^2 + \frac{D}{U}\frac{h_{,n}}{F_0^2}, \quad (3.6)$$

having used flow continuity and assumed the following slowly varying structure of the eddy viscosity:

$$v_T = UD\mathcal{N}(\zeta). \tag{3.7}$$

The solution for v_0 and h_0 can then be determined by means of an iterative procedure. We assume, as a first approximation, that secondary flow is in phase with curvature, and neglect in equation (3.6) the convective term and the topographic term originating from the coordinate transformation. We then readily find

$$v_0 = \frac{DU}{\beta\sqrt{C_{f0}}}\mathcal{C}(s)\mathcal{G}_0(\zeta), \tag{3.8}$$

$$h_{,n} = v_0 h_{0,n} = v_0 \frac{F_0^2 U^2 \mathcal{C}(s)a_0}{\beta\sqrt{C_{f0}}}, \tag{3.9}$$

where the function $\mathcal{G}_0(\zeta)$ (describing the vertical distribution of secondary flow) and the constant a_0 (describing the transverse slope of the free surface) satisfy the following differential system with $i = 0$:

$$[\mathcal{N}\mathcal{G}_{i,\zeta}]_{,\zeta} = \mathcal{P}_i(\zeta); \tag{3.10}$$

$$\mathcal{G}_i|_{\zeta_0} = \mathcal{G}_{i,\zeta}|_{\zeta=1} = 0, \quad \int_{\zeta_0}^{1}\mathcal{G}_i \, d\zeta = 0; \tag{3.11}$$

$$\mathcal{P}_0(\zeta) = a_0 - \mathcal{F}_0^2(\zeta), \quad \mathcal{P}_1(\zeta) = \mathcal{F}_0\mathcal{G}_0 + a_1, \quad \mathcal{P}_2(\zeta) = (1-\zeta)\mathcal{F}_0\mathcal{G}_{0,\zeta} - a_2. \tag{3.12}$$

The reader may have noticed that the structure of secondary flow, as given by (3.6), adapts the classical solution for secondary flow in constant-curvature channels to channels with arbitrary curvature distribution.

Once the function $\mathcal{G}_0$ and the constant a_0 are determined, we may proceed to evaluate the corrections induced on v_0 and $h_{0,n}$ by longitudinal convection and shoaling effects (first and second term in the right-hand side of (3.6)). We readily find that such corrections may be given a similarity structure of the form

$$v_0 = \frac{DU}{\beta\sqrt{C_{f0}}}\mathcal{C}(s)\mathcal{G}_0(\zeta) + \frac{D^2}{\beta^2 C_{f0}}(U\mathcal{C})_{,s}\mathcal{G}_1(\zeta) + \frac{DU}{\beta^2 C_{f0}}\mathcal{C}D_{,s}\mathcal{G}_2(\zeta), \tag{3.13}$$

$$h_{0,n} = \frac{UF_0^2}{\beta\sqrt{C_{f0}}}[Ua_0\mathcal{C}(s) + Ua_1(D\mathcal{C})_{,s} + Da_2\mathcal{C}U_{,s}], \tag{3.14}$$

where the vertical distribution of the corrections of secondary flow, namely the functions $\mathcal{G}_1(\zeta)$ and $\mathcal{G}_2(\zeta)$, and the constants a_1, a_2 are solutions of the ordinary differential problems (3.10)–(3.12) where $i = 1$ and $i = 2$, respectively.

The procedure could be extended to a higher approximation, at least in principle. Provided curvature is slowly varying in space, such effort is not worthwhile as the level of algebraic complexity would rapidly become prohibitive.

The functions $\mathcal{G}_0$, $\mathcal{G}_1$ and $\mathcal{G}_2$ and the constants a_0, a_1 and a_2 have been calculated,
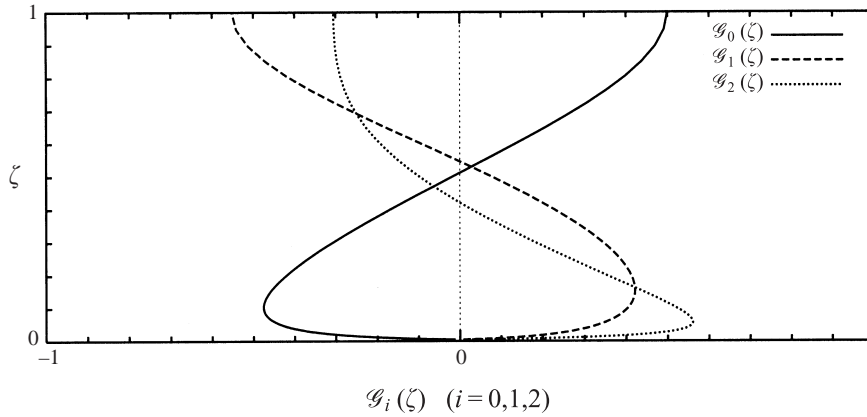
$$\mathcal{G}_i(\zeta) \quad (i = 0, 1, 2)$$

FIGURE 2. Vertical distributions of the functions $\mathcal{G}_0(\zeta)$, $\mathcal{G}_1(\zeta)$ and $\mathcal{G}_2(\zeta)$ describing the various components of secondary flow. The value of the friction coefficient C_{f0} has been assumed to be equal to 0.008.

solving each of the differential systems analytically in terms of solutions of initial-value problems obtained numerically. The procedure is identical with that employed by Seminara & Solari (1998). In the calculations we have assumed the following form for $\mathcal{N}(\zeta)$ (Dean 1974):

$$\mathcal{N}(\zeta) = \frac{k(\zeta)(1 - \zeta)}{1 + 2A\zeta^2 + 3B\zeta^3}, \tag{3.15}$$

hence, $\mathcal{F}_0(\zeta)$ reads:

$$\mathcal{F}_0 = \frac{\sqrt{C_{f0}}}{k} \left[\ln \frac{\zeta}{\zeta_0} + A(\zeta^2 - \zeta_0^2) + B(\zeta^3 - \zeta_0^3) \right], \tag{3.16}$$

with $A = 1.84$ and $B = -1.56$.

The solutions for $\mathcal{G}_0(\zeta)$, $\mathcal{G}_1(\zeta)$ and $\mathcal{G}_2(\zeta)$ are plotted in figure 2.

Notice that the signs of both $\mathcal{G}_1$ and $\mathcal{G}_2$ are opposite to the sign of $\mathcal{G}_0$. Hence, equation (3.13) suggests that the centrifugally induced secondary flow is damped in reaches where curvature and/or longitudinal velocity and/or flow depth experience growth and vice versa.

4. A depth-averaged model for flow in meandering rivers

We now substitute from the decomposition (3.1)–(3.3) and the solution (3.13) and (3.14) into the governing differential problem (2.2)–(2.4) written in terms of the normalized variable ζ, and perform a depth integration.

In order to clarify the procedure let us consider a typical convective term of the three-dimensional equations, say the left-hand side of (2.2). Substituting from (3.3) and (3.1) into such a term, performing depth averaging and recalling the kinematic conditions both at the bed and at the free surface we find:

$$N I_{uu,s} + \left(\frac{\partial}{\partial n} + 2v_0 N \mathcal{C} \right) I_{uv}, \tag{4.1}$$

$$I_{uu} = DU^2, \quad I_{uv} = DUV + v_0 \varphi_0(s, n),$$

$$\varphi_0(s, n) = DU \int_{\zeta_0}^{1} v_0(\zeta, n, s) \mathcal{F}_0(\zeta) \, d\zeta, \tag{4.2}$$

as $\int_{\zeta_0}^{1} \mathcal{F}_0(\zeta) \, d\zeta \simeq 1$.

The function $\varphi_0(s,n)$ involves the redistribution coefficients k_0, k_1 and k_2, defined by (4.15), and takes the form:

$$\varphi_0(s,n) = \frac{DU}{\beta\sqrt{C_{f0}}}\left[DU\mathscr{C}(k_0 + k_2 D_{,s}) + k_1\frac{D^2(U\mathscr{C})_{,s}}{\beta\sqrt{C_{f0}}}\right]. \qquad (4.3)$$

Taking into account the depth averaged form of the continuity equation, the left-hand side of (2.2) then gives:

$$UU_{,s} + VU_{,n} + v_0\varphi_1(s,n) + v_0^2\varphi_2(s,n), \qquad (4.4)$$

$$\varphi_1(s,n) = \frac{\varphi_{0,n}}{ND} + V\mathscr{C}(s)[nU_{,n} + U], \qquad \varphi_2(s,n) = 2\mathscr{C}(s)\frac{\varphi_0}{D}. \qquad (4.5)$$

The function $\varphi_1(s,n)$ contributes to the term f_{11}, whose expression is reported in Appendix A, and $\varphi_2(s,n)$ is part of $O(v_0^2)$ terms which will be neglected in the context of the present linear theory.

We do not pursue the derivation of the depth-averaged form of all equations which would require a considerable amount of tedious algebra. The latter eventually leads to the following modified shallow-water equations for the average quantities U, V, H, D coupled with the two-dimensional form of the Exner equation:

$$UU_{,s} + VU_{,n} + H_{,s} + \beta\frac{\tau_s}{D} = v_0 f_{11} + O(v_0^2), \qquad (4.6)$$

$$UV_{,s} + VV_{,n} + H_{,n} + \beta\frac{\tau_n}{D} = v_0 g_{11} + O(v_0^2), \qquad (4.7)$$

$$(DU)_{,s} + (DV)_{,n} = v_0 m_{11}, \qquad (4.8)$$

$$(F_0^2 H - D)_{,t} + Q_0[q_{s,s} + q_{n,n}] = v_0 n_{11}. \qquad (4.9)$$

In equations (4.6)–(4.9), H is a free-surface elevation which may be written as follows:

$$H = \frac{h}{F_0^2} - \beta C_{f0}s, \qquad (4.10)$$

where h is given by (3.2). Moreover, τ_s and τ_n are the components of the bottom stress vector. Employing the decomposition (3.1) and the solutions for $\mathscr{G}_0, \mathscr{G}_1$ and $\mathscr{G}_2$ we find:

$$(\tau_s, \tau_n') = C_f(U,V)|U|, \quad |U| = (U^2 + V^2)^{1/2}, \quad \tau_n = \tau_n' + \tau_H, \qquad (4.11)$$

$$\tau_H = v_0 C_f|U|\left[\frac{DU\mathscr{C}}{\beta\sqrt{C_{f0}}}\left(k_3 + \frac{D_{,s}}{\beta\sqrt{C_{f0}}}k_5\right) + \frac{D^2(U\mathscr{C})_{,s}}{\beta^2 C_{f0}}k_4\right]. \qquad (4.12)$$

Here k_3, k_4 and k_5 are defined by the relationships:

$$k_3 = \left.\frac{\mathscr{G}_{0,\zeta}}{\mathscr{F}_{0,\zeta}}\right|_{\zeta_0}, \quad k_4 = \left.\frac{\mathscr{G}_{1,\zeta}}{\mathscr{F}_{0,\zeta}}\right|_{\zeta_0}, \quad k_5 = \left.\frac{\mathscr{G}_{2,\zeta}}{\mathscr{F}_{0,\zeta}}\right|_{\zeta_0}. \qquad (4.13a\text{--}c)$$

Finally, Q_0 is a dimensionless parameter defined as

$$Q_0 = \frac{\sqrt{(s-1)gd_s^{*3}}}{(1-p)U_0^* D_0^*}, \qquad (4.14)$$

and q_s and q_n are obtained from (2.13) and (2.14) by deriving the form of the matrix **G** in the (s,n) reference frame through a simple linear transformation.
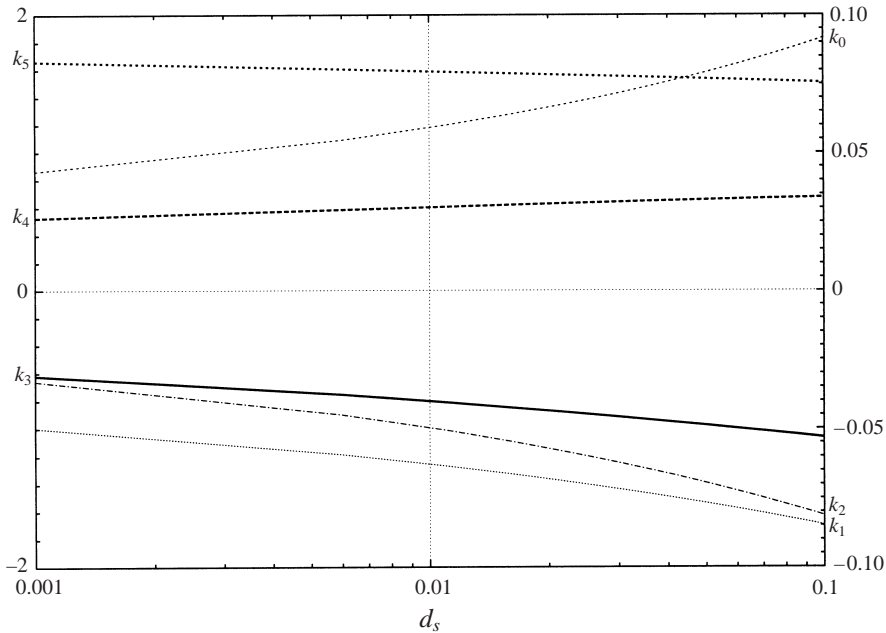
FIGURE 3. Dependence of the dispersive coefficients k_0–k_5 on the relative roughness d_s. The scale for k_0–k_2 is given on the right-hand vertical axis. The scale for k_3–k_5 is given on the left-hand vertical axis.

The quantities f_{11}, g_{11}, m_{11} and n_{11} which appear in the right-hand sides of equations (4.6)–(4.9) are given in Appendix A. They involve the coefficients k_0, k_1 and k_2 which account for the dispersive effects due to the nonlinear interactions between the centrifugal and topographic components of secondary flow. The coefficients k_0, k_1 and k_2 read:

$$k_i = \int_{\zeta_0}^{1} \mathscr{F}_0 \mathscr{G}_i \, \mathrm{d}\zeta \quad (i = 0, 1, 2). \tag{4.15}$$

The dependence of the coefficients k_0–k_5 on the relative roughness d_s is plotted in figure 3. The boundary conditions to be associated with equations (4.6)–(4.9) impose that the lateral walls must be impermeable both to fluid and to sediments, hence:

$$V = q_n = 0 \quad (n = \pm 1). \tag{4.16}$$

Furthermore, boundary conditions must be imposed at the upstream and downstream end cross-sections. They are discussed in §5 in relation to the problem of upstream and downstream influence in river morphodynamics.

We note that the above formulation is fully nonlinear. In this respect, it generalizes previous formulations adopted in linear (Johannesson & Parker 1989) as well as weakly nonlinear contexts (Tubino & Seminara 1990; Seminara & Tubino 1992). However, note that the centrifugal component of the secondary flow enters the formulation through its significant effect on bottom stress (see equation (4.12)). On the contrary, the redistribution coefficients k_0, k_1 and k_2 are sufficiently small to justify neglecting momentum redistribution in the governing equations (4.6)–(4.9).

In the next section, we derive the linearized form of the problem formulated above and solve it exactly for an arbitrary distribution of channel curvature.

5. The linearized form of the problem of river morphodynamics

We now assume that flow and topography perturbations originating either from deviations of the channel configuration from the straight configuration or from the existence of non-uniform end conditions are small enough to allow for linearization of the mathematical problem formulated in §4. We note that this is a fairly restrictive assumption. However, the recent contribution of Seminara & Solari (1998) referring to constant-curvature channels suggests that linearity is likely to be a reasonable approximation, at least in the case of dominant bedload, as long as the parameter $(v_0\sqrt{\tau_*}/rC_{f0})$ attains values which do not exceed roughly 10. Moreover, a linear theory fulfils various other aims. First, it allows for an analytical solution which clarifies the fundamental issue of upstream and downstream influence in the morphodynamics of meandering rivers, which is the main subject of the present paper. Secondly, a linear solution can be set as the basis of a fully nonlinear treatment of the problem the solution of which may be obtained by successive approximations.

Let us then set:

$$(U, V, D, H) = (U_0, 0, D_0, H_0) + v_0(u, v, d, h) + O(v_0^2). \tag{5.1}$$

Furthermore, assuming that perturbations superimpose on a uniform flow configuration (a useful but inessential assumption), we may set

$$(U_0, 0, D_0, h_0) = (1, 0, 1, h_0), \tag{5.2}$$

where the reader will note that quantities are scaled by their uniform counterparts.

Substituting from (5.1) and (5.2) into (4.6)–(4.9) and retaining only linear terms in the perturbation parameter v_0, with the help of some algebraic manipulation we derive the following linear system of partial differential equations:

$$\left(\frac{\partial}{\partial s} + a_1\right)u + \frac{\partial h}{\partial s} + a_2 d = nb_1\mathscr{C}(s), \tag{5.3}$$

$$\left(\frac{\partial}{\partial s} + a_3\right)v + \frac{\partial h}{\partial n} = b_2\mathscr{C}(s) + b_3\mathscr{C}'(s) + b_5\mathscr{C}''(s), \tag{5.4}$$

$$\frac{\partial u}{\partial s} + \frac{\partial v}{\partial n} + \frac{\partial d}{\partial s} = 0, \tag{5.5}$$

$$a_4\frac{\partial u}{\partial s} + \frac{\partial v}{\partial n} + \left(a_5\frac{\partial}{\partial s} + a_6\frac{\partial^2}{\partial n^2}\right)d - F_0^2 a_6\frac{\partial^2 h}{\partial n^2} = 0, \tag{5.6}$$

with boundary conditions

$$v = 0 \quad (n = \pm 1), \tag{5.7}$$

$$(F_0^2 h - d)_{,n} = b_4\mathscr{C}(s) + b_6\mathscr{C}'(s) \quad (n = \pm 1). \tag{5.8}$$

The coefficients $a_1 - a_6$ and $b_1 - b_6$ in equations (5.3)–(5.8) read:

$$a_1 = \frac{2\beta C_{f0}}{1 - C_{fT}}, \quad a_2 = \beta C_{f0}\left(\frac{C_{fD}}{1 - C_{fT}} - 1\right), \quad a_3 = \beta C_{f0}, \tag{5.9a–c}$$

$$a_4 = \frac{2\Phi_T}{1 - C_{fT}}, \quad a_5 = \Phi_D + \frac{C_{fD}\Phi_T}{1 - C_{fT}}, \quad a_6 = \frac{r}{\beta\sqrt{\tau_{*0}}}, \tag{5.9d–f}$$

$$b_1 = -\beta C_{f0}, \quad b_2 = 1 - \sqrt{C_{f0}}k_3, \quad b_3 = -\frac{k_0}{\beta\sqrt{C_{f0}}} - \frac{k_4}{\beta}, \qquad (5.9g\text{–}i)$$

$$b_4 = \frac{k_3\sqrt{\tau_{*0}}}{r\sqrt{C_{f0}}}, \quad b_5 = -\frac{k_1}{\beta^2 C_{f0}}, \quad b_6 = \frac{k_4\sqrt{\tau_{*0}}}{\beta C_{f0}r}, \qquad (5.9j\text{–}l)$$

where

$$C_{fD} = \frac{C_{f,D}|_0}{C_{f0}}, \quad C_{fT} = \frac{\tau_{*0}}{C_{f0}}C_{f,\tau_*}|_0, \quad \Phi_D = \frac{\Phi_{,D}|_0}{\Phi_0}, \quad \Phi_T = \frac{\tau_{*0}}{\Phi_0}\Phi_{,\tau_*}|_0. \qquad (5.10a\text{–}d)$$

In the above equations, the subscript 0 refers to the uniform equilibrium conditions and the approach implicitly assumes that both the friction coefficient and the intensity of bedload transport can be evaluated in terms of local values of flow and sediment parameters, a quasi-equilibrium assumption which is justified by the slowly varying character of both flow field and sediment dynamics.

The above linear system of partial differential equations can be easily transformed into a linear system of ordinary differential equations. It is first convenient to perform the following decomposition:

$$(u,v,h,d) = [0,0,(\bar{h}_1\mathscr{C} + \bar{h}_2\mathscr{C}' + \bar{h}_3\mathscr{C}''),(\bar{d}_1\mathscr{C} + \bar{d}_2\mathscr{C}' + \bar{d}_3\mathscr{C}'')]n + (\hat{u},\hat{v},\hat{h},\hat{d}), \qquad (5.11)$$

with

$$\bar{h}_1 = b_2, \quad \bar{h}_2 = b_3, \quad \bar{h}_3 = b_5, \quad \bar{d}_1 = F_0^2\bar{h}_1 - b_4, \quad \bar{d}_2 = F_0^2\bar{h}_2 - b_6, \quad \bar{d}_3 = F_0^2\bar{h}_3.$$

$$(5.12a\text{–}f)$$

This enables us to transform the original system into a linear non-homogeneous partial differential system with homogeneous boundary conditions for the functions $\hat{u},\hat{v},\hat{h}$ and $\hat{d}$. We then remove the partial differential character of the governing differential problem by expanding the dependent variables in Fourier series as follows:

$$(\hat{u},\hat{h},\hat{d}) = \sum_{m=0}^{\infty}(u_m,h_m,d_m)\sin(Mn), \quad \hat{v} = \sum_{m=0}^{\infty}v_m\cos(Mn), \qquad (5.13a,b)$$

where

$$M \equiv \tfrac{1}{2}(2m+1)\pi. \qquad (5.14)$$

Note that the boundary conditions at $n = \pm 1$ are satisfied by the latter expansions which also respect the symmetric character of v and the antisymmetric character of u,h and d. By substituting from (5.11)–(5.13) into the system (5.3)–(5.8), straightforward algebraic manipulations lead to a system of four ordinary differential equations with constant coefficients, which can be solved in cascade, for each of the Fourier components. We find:

$$\left(\sigma_4\frac{d^4}{ds^4} + \sigma_3\frac{d^3}{ds^3} + \sigma_2\frac{d^2}{ds^2} + \sigma_1\frac{d}{ds} + \sigma_0\right)u_m = -A_m\sum_{j=0}^{6}\varrho_{j+1}\frac{d^{(j)}\mathscr{C}}{ds^{(j)}} \quad (m=0,1,2,\dots),$$

$$(5.15)$$

$$(d_m,v_m,h_m) = \sum_{j=1}^{4}(d_{mj},v_{mj},h_{mj})\frac{d^{(j-1)}u_m}{ds^{(j-1)}} + A_m\sum_{j=5}^{9}(d_{mj},v_{mj},h_{mj})\frac{d^{(j-5)}\mathscr{C}}{ds^{(j-5)}}, \qquad (5.16)$$

G. Zolezzi and G. Seminara

where

$$A_m = (-1)^m \frac{2}{M^2}, \qquad (5.17)$$

while the coefficients $\sigma_{0-4}, \varrho_{1-7}, d_{mj}, v_{mj}, h_{mj}(j = 1\text{--}9)$ are reported in Appendix B (held in an editorial file).

The latter system of ordinary differential equations in the longitudinal coordinate must be supplemented by suitable boundary conditions, the nature of which will be clarified in the next section where we derive the exact solution of the problem.

6. The exact solution of the linear problem of meander morphodynamics

The differential system (5.15) and (5.16) can be solved in closed form. Though the derivation is somewhat tedious algebraically, this solution allows us to clarify the problem of morphodynamic influence in erodible channels and provides a tool which is readily amenable to numerical implementation.

Equation (5.15) is a non-homogeneous ordinary differential equation with constant coefficients which can be solved using the so-called method of variation of parameters (see Coddington & Levinson 1955, p. 75). Once the solution for u_m is known, then we can solve for the remaining dependent variables by employing equation (5.16). The exact solution of the linear problem of meander morphodynamics can then be written in the form:

$$(u_m, v_m, d_m, h_m) = \sum_{j=1}^{4} \left\{ (1, \varphi_{mj}, \delta_{mj}, \xi_{mj}) \left[\hat{A}_m g_{j0} \int_{s0}^{s} \exp \lambda_{mj}(s - t) \mathscr{C}(t) \, \mathrm{d}t \right. \right.$$
$$\left. \left. + c_{mj} \exp \lambda_{mj}(s - s_0) \right] + \hat{A}_m \sum_{k=1}^{9} \Gamma_{jk}^{(u,v,d,h)} \frac{\partial^{(k-1)} \mathscr{C}}{\partial s^{(k-1)}} \right\}. \qquad (6.1)$$

In the latter relationship, $c_{mj}(j = 1, \ldots, 4; m \geqslant 1)$ are constants to be determined and $\hat{A}_m = A_m/\sigma_4$. Furthermore,

$$(\delta_{mj}, \varphi_{mj}, \xi_{mj}) = \sum_{\ell=1}^{4} (d_{m\ell}, v_{m\ell}, h_{m\ell})(\lambda_{mj})^{\ell-1}, \qquad (6.2)$$

$$\Gamma_{jk}^{(u)} = g_{jk} \quad (j = 1, \ldots, 4, k = 1, \ldots, 6), \quad \Gamma_{jk}^{(u)} = 0 \quad (k > 6), \qquad (6.3)$$

$$(\Gamma_{jk}^{(d)}, \Gamma_{jk}^{(v)}, \Gamma_{jk}^{(h)}) = \Gamma_{jk\ell}(d_{m\ell}, v_{m\ell}, h_{m\ell}) \quad (m \geqslant 1, k = 1, \ldots, 9), \qquad (6.4)$$

where the subscript ℓ in equation (6.4) is summed and the elements of the matrices g_{jk} and $\Gamma_{jk\ell}$ have the form reported in Appendix C (held in an editorial file).

The characteristic exponents $\lambda_{mj}(j = 1, \ldots, 4)$ for each mode m play a fundamental role in the analysis. They were first investigated by Olesen (1983) and were later reexamined by Struiksma et al. (1985) and Seminara & Tubino (1992) in different contexts. These investigations have shown that one of the exponents is invariably real and positive, one is real and negative, the last two are complex conjugates. The real part of the complex exponents is negative, provided the dimensionless parameter β does not exceed a threshold value which, for the first mode, coincides with the resonant value β_R of Blondeaux & Seminara (1985). For the higher modes, it is easy to show that $\beta_R^{(m)}$ is m times β_R. Figure 4 provides an example of the dependence of the real and imaginary parts of the characteristic exponents of the first mode on

the aspect ratio β for given values of τ_* and d_s. For the higher modes, the following relationship holds:

$$\lambda_{mj}(\beta;\tau_*,d_s) = m\lambda_{1j}\left(\frac{\beta}{m};\tau_*,d_s\right) \quad (m > 1). \qquad (6.5)$$

The latter results have a direct consequence on the problem of upstream and downstream morphodynamic influence.

In order to clarify this, we first point out that the constants $c_{mj}(j = 1,4)$ which appear in (6.1) must obviously be chosen such as to fit the boundary conditions at the upstream and downstream ends of the reach being investigated.

Let us consider the sub-resonant case ($\beta < \beta_R^m$, $m \geqslant 1$) and let λ_{m1} denote the real positive characteristic exponent. In this case, for each mode m, one of the boundary conditions must be imposed at the downstream end while the remaining three must be assigned at the upstream end. With the help of some algebraic manipulations equation (6.1) then takes the following form:

$$(u_m, v_m, d_m, h_m) = \underbrace{-\hat{A}_m g_{10}(1, \varphi_{m1}, \delta_{m1}, \xi_{m1}) \int_s^{s_0+L} \exp{-\lambda_{m1}(t-s)}\mathscr{C}(t)\,\mathrm{d}t}_{1-\text{ upstream propagating influence}}$$

$$\underbrace{+\hat{A}_m \sum_{j=2}^{4} g_{j0}(1, \varphi_{mj}, \delta_{mj}, \xi_{mj}) \int_{s0}^{s} \exp{\lambda_{mj}(s-t)}\mathscr{C}(t)\,\mathrm{d}t}_{2-\text{ downstream propagating influence}}$$

$$\underbrace{+\hat{A}_m \sum_{j=1}^{4} \left[\sum_{k=1}^{9}(\Gamma_{jk}^{(u)}, \Gamma_{jk}^{(v)}, \Gamma_{jk}^{(d)}, \Gamma_{jk}^{(h)})\frac{\partial^{(k-1)}\mathscr{C}}{\partial s^{(k-1)}}\right]}_{3-\text{ local effect}}$$

$$\underbrace{+u_m|_{s_0+L}(1, \varphi_{m1}, \delta_{m1}, \xi_{m1})\exp{-\lambda_{m1}(s_0+L-s)}}_{4-\text{ upstream effect of downstream boundary condition}}$$

$$\underbrace{+\sum_{j=2}^{4}(1, \varphi_{mj}, \delta_{mj}, \xi_{mj})c_{mj}\exp{\lambda_{mj}(s-s_0)}}_{5-\text{ downstream effect of upstream boundary condition}}. \qquad (6.6)$$

The constants $c_{mj}(j = 2,3,4)$ are readily obtained once the boundary conditions to be imposed at $s = s_0$ are known. The different contributions in the right-hand side of equation (6.6) interpret the various effects which determine the morphodynamics of a meandering river at a given cross-section. They may be described as follows.

(i) Contribution *1* (single contribution in the sub-resonant case) accounts for the morphodynamic influence of the downstream reach on the given cross-section.

(ii) Contribution *2* (three contributions in the sub-resonant case) accounts for the similar morphodynamic influence of the upstream reach on the given cross-section.

(iii) Contribution *3* interprets how the local channel curvature and its variations in a neighbourhood of the given cross-section contribute to determine the morphodynamic asset of the latter.
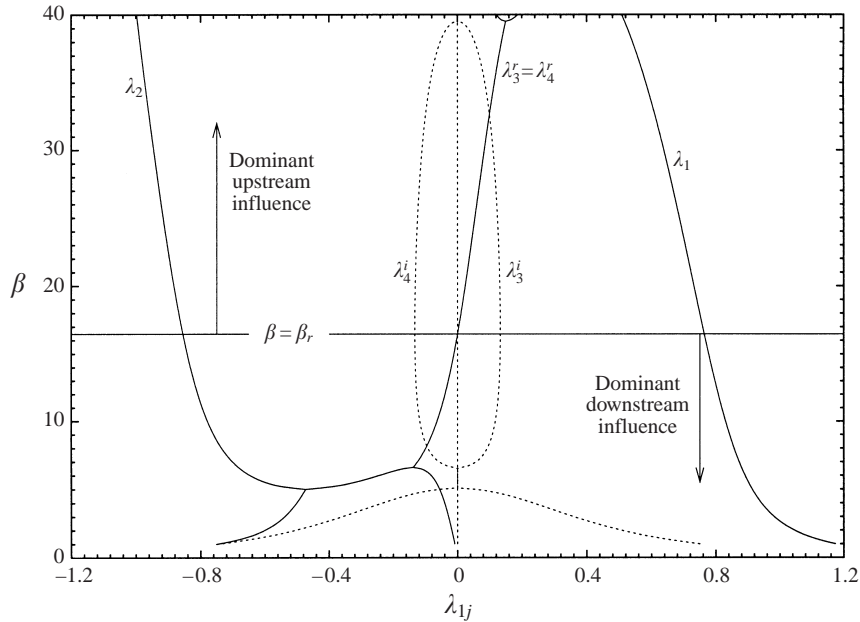
FIGURE 4. The four characteristic exponents $\lambda_{mj}(j = 1\text{–}4)$ for the first mode are plotted versus the dimensionless parameter β (half-width to depth ratio) for given values of Shields stress ($\tau_* = 0.1$) and relative roughness ($d_s = 0.01$) for the plane bed case. Solid lines denote the real parts of the exponents while dotted lines denote their imaginary parts.

(iv) Contribution *4* describes the effect of the boundary conditions at the downstream end on the reach under investigation.

(v) Contribution *5* describes the effect of the boundary conditions at the upstream end on the reach under investigation.

The regions of influence of the different contributions are schematically described in figure 1. Note that we have assumed that the reach is long enough for the effect of the downstream boundary conditions to be negligible at the upstream end and vice versa. Otherwise, the evaluation of the constants $c_{mj}(j = 2, 3, 4)$ in $s = s_0$ would be coupled with the evaluation of the constant c_{m1} in $s = s_0 + L$.

Let us analyse the structure of the exact solution (6.6) with the aim of clarifying the issue of morphodynamic influence. Recalling figure 4, it appears that the real part of λ_{m1} is an order one number. Hence, in the sub-resonant case, the effect of contributions *1* and *4* damps out within a distance of the order of a few channel widths. Moreover, of the three contributions *2*, one is also damped very fast while the remaining two affect a reach of length of the order of a few tenths of the channel width, a length which increases in a neighbourhood of the resonant conditions, reaching a theoretically infinite distance exactly at resonance. The latter scenario may be summarized by stating that under sub-resonant conditions the morphodynamic influence is felt dominantly downstream.

The latter picture is reversed when the channel falls in the super-resonant regime, at least as far as the first mode is concerned. Under these conditions the solution for the higher sub-resonant modes is still in the form of equation (6.6), as $\beta_R^m = m\beta_R$. On the contrary, the first, super-resonant, mode, which typically provides the dominant contribution to the morphodynamics, exhibits an upstream influence arising from the presence of three contributions of type *1*, one of them being purely damped

at a fast rate while the other two are oscillatory and weakly damped. A weak downstream influence is also displayed by super-resonant modes through the single contribution of type *2* which is now strongly damped downstream. Similarly, the number of contributions of types *4* and *5* is also reversed. This second scenario may be summarized by stating that the morphodynamic influence concerning super-resonant modes is felt dominantly upstream. The latter result does not appear to have been previously noted, though it was essentially implied by the work of Olesen (1983) and Struiksma *et al.* (1985).

7. A physical explanation of the occurrence of upstream influence

Results obtained in the last section naturally suggest that, under super-resonant conditions, information concerning the development of two-dimensional perturbations of bottom topography may propagate upstream. This can be given a physical explanation on the basis of the classical linear stability analysis employed to investigate the occurrence of free bars in a straight channel (e.g. Colombini, Seminara & Tubino 1987). In Colombini *et al.*, the growth of small-amplitude perturbations of the flow field and bottom topography with respect to a basic state consisting of a uniform flow over a plane bed in a straight channel was examined. The longitudinal and temporal structure of the mth mode of the perturbation of bottom topography η_m can be put in the form

$$\eta_m(s, n, t) = \eta_r \exp(\Omega t) \cos(\lambda s - \omega t) \sin(\tfrac{1}{2}\pi mn), \tag{7.1}$$

where η_r is a real positive quantity, t is dimensionless time and Ω, λ and ω are real numbers representing growth rate, dimensionless wavenumber and angular frequency of the perturbation, respectively.

The above analysis, involving the homogeneous component of the system (5.3)–(5.6), reveals that bar formation is controlled by a delicate balance between destabilizing and stabilizing effects, that are associated with the divergence of the perturbed bedload discharge vector, whose longitudinal and transverse components can be expressed in the following form:

$$\left. \begin{array}{l} Q_{s1} = Q_{sr} \exp(\Omega t) \cos(\lambda s - \omega t - \delta_1) \sin(\tfrac{1}{2}\pi mn), \\[2mm] Q_{n1} = Q_{nr} \exp(\Omega t) \cos(\lambda s - \omega t - \delta_2) \cos(\tfrac{1}{2}\pi mn), \end{array} \right\} \tag{7.2}$$

with Q_{sr} and Q_{nr} real positive quantities and δ_1 and δ_2 phase lags, relative to bed profile, of the perturbations of the longitudinal and transverse bedload discharge, respectively.

The main output of the above linear stability analysis consists of the neutral curve for bar stability ($\Omega = 0$), which is reported in figure 5 together with the neutral curve for bar migration ($\omega = 0$).

The first major implication of figure 5 is that the point of intersection of the marginal stability curve and of the curve characterized by vanishing angular frequency defines the resonant conditions (λ_R, β_R) of Blondeaux & Seminara (1985). The dependence of β_R and λ_R on the Shields stress and the relative roughness d_s is plotted in figure 6, where Engelund & Hansen's (1967) formula has been employed and the presence of dunes has been assumed. A similar plot for the flat bed case is reported in Seminara & Tubino (1992) (figures *2a* and *3a*, pp. 265 and 266), where the Meyer-Peter and Muller's formula, in the form given by Chien (1956) has been employed. Are the values of β_R realistic? Figure 7 answers this question. We have plotted data concerning a number of meandering gravel bed rivers of Colorado (Andrews 1984)

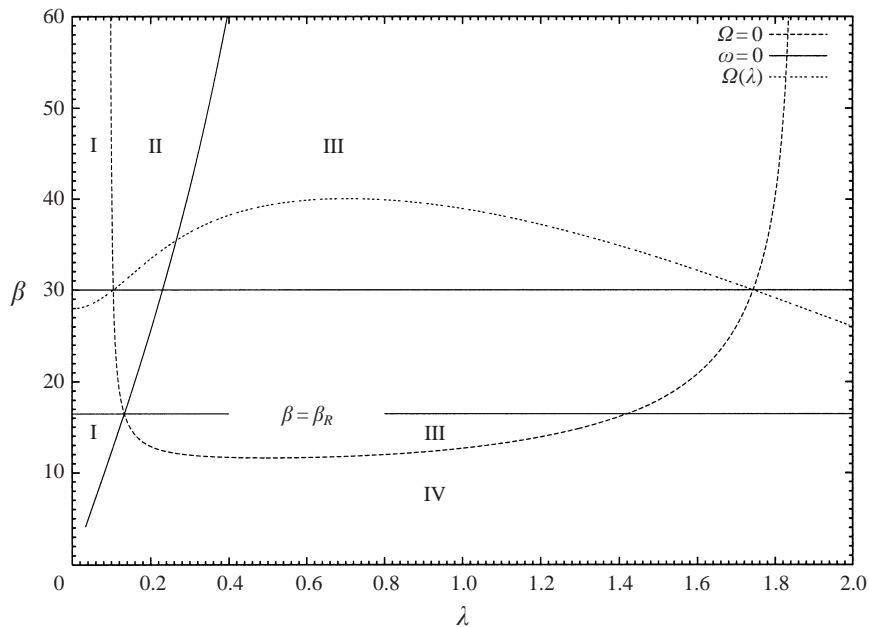FIGURE 5. Neutral curves for two-dimensional free bars instability ($\Omega = 0$) and migration ($\omega = 0$), dividing the (λ, β)-plane in the four different regions I to IV. The additional dashed line in the middle of the plot shows the qualitative behaviour of $\Omega(\lambda)$ for a given $\beta > \beta_R$ (plane bed, $\tau_* = 0.1$, $d_s = 0.01$).

and Minnesota (MacDonald, Parker & Leuthe 1991) (USA), Alberta (Kellerhals, Neill & Bray 1972) and British Columbia (courtesy of G. Parker) (Canada). It appears that under bedload dominated conditions both sub- and super-resonant regimes are frequently encountered in nature.

The significance of resonant conditions in terms of actual physical processes related to river meandering arises from the facts discussed below.

(*a*) Resonant bar perturbations are essentially non-migrating and non-amplifying (hence steady) periodic perturbations of flow and bed topography naturally allowed by the system flow-cohesionless bottom: if the channel centreline meanders with wavenumber λ_R (or close to it) and the aspect ratio of the channel is β_R (or close to it), then the forcing effect of curvature (right-hand sides of (5.3)–(5.8)) is such as to force a free response of the system (i.e. a solution of the homogeneous part of the problem (5.3)–(5.8)) and the system resonates, i.e. flow and bottom perturbations peak, at least in a linear context. Though exact resonant conditions would never be met in nature, however, the above finding allowed Blondeaux & Seminara (1985) to clarify the fundamental difference between the two distinct theories of meander formation, namely, the so called bar and bend theories. In particular, such theories select markedly different wavenumbers: the bar mechanism selects the most unstable bar perturbations (a migrating feature), whereas the bend theory selects the wavenumber such that the (steady) perturbation of flow and bed topography forced by curvature is most intense. The latter would be exactly the resonant wavenumber λ_R if the aspect ratio of the channel were exactly β_R, but even for values of β significantly larger or smaller than β_R, resonance displays its effects in that a peak in the response of bed topography to a periodic perturbation of channel axis is found for values of meander wavenumber fairly close to λ_R. In other words, the peak of the bend theory
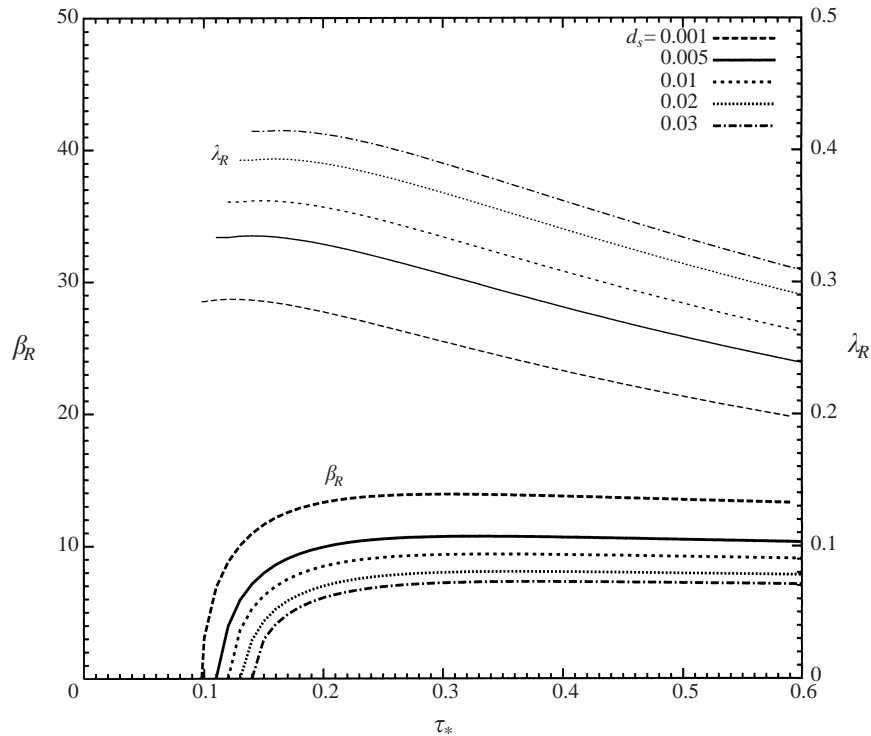
FIGURE 6. The resonant values of width ratio β_R and wavenumber λ_R are plotted versus the Shields stress τ_* for different values of the relative roughness d_s in the case of a dune-covered bed.

originally proposed by Ikeda *et al.* (1981) is associated with the fact that the bend mechanism selects a quasi-resonant wavenumber. Such findings have been confirmed by Johannesson & Parker (1989) and by Hasegawa, Nakamura & Toyabe (1998). Nonlinear effects obviously smooth out the sharpness of the resonant response. This has been shown analytically by Seminara & Tubino (1992), numerically by Shimizu, Tubino & Watanabe (1992) and experimentally by Colombini, Tubino & Whiting (1992) and Hasegawa *et al.* (1998).

(*b*) A second physical implication of the existence of such resonant conditions concerns the location of the maximum scour in a meandering channel. In mathematical terms, this has to do with the phase of the perturbation of bottom topography arising in response to perturbations of channel curvature. A well-known feature of linear resonators is the change in phase of the response as the resonant conditions are crossed (Kevorkian & Cole 1981, p. 145). In the present case, under sub-resonant conditions ($\beta < \beta_R$) the location of the maximum scour moves from downstream to upstream of the bend apex as the wavenumber increases exceeding λ_R. The situation reverses under super-resonant conditions ($\beta > \beta_R$): the location of the maximum scour is located upstream (downstream) of the bend apex for values of λ smaller (larger) than λ_R. Such a result, which has been experimentally confirmed by Colombini *et al.* (1992), Hasegawa *et al.* (1998) and Garcia & Nino (1993) independently, besides its obvious practical implications has an important consequence as regards the well-known process of skewing of the shape of large-amplitude meanders: in fact, meanders are skewed upstream or downstream depending on whether the location of maximum scour is downstream or upstream of the bend apex. As a result, sub- (super-)resonant
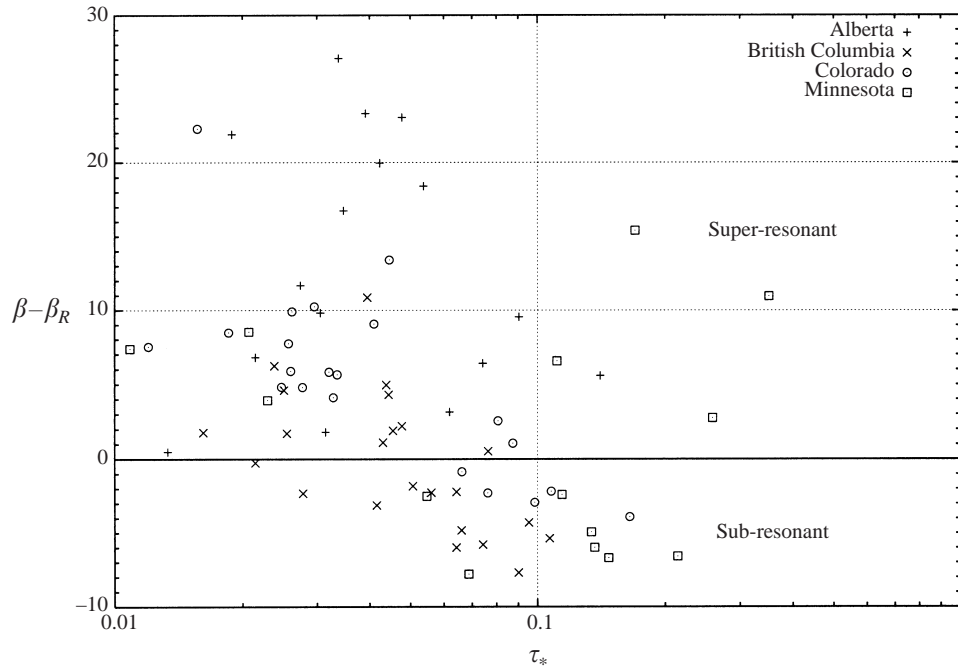
FIGURE 7. The difference $\beta - \beta_R$ for several North American gravel bed rivers is plotted versus the Shields stress τ_*. Data partly taken from MacDonald *et al.* (1991), Kellerhals *et al.* (1972), Andrews (1984), partly provided by G. Parker.

large-amplitude meanders are downstream or upstream skewed, respectively. This feature will clearly be demonstrated in Part 2.

(*c*) The third important implication of the existence of resonant conditions concerns upstream influence in river meandering. Let us then clarify the physical basis of our findings.

Figure 5 shows that the (λ, β)-plane can be divided into four different regions according to the signs of the growth rate Ω and of the angular speed ω of the perturbation. Alternate bars do not form in regions I and IV, characterized by a negative value of the growth rate Ω. The instability area covers both regions II and III, characterized by different signs for the angular speed ω. Region II displays upstream migration ($\omega < 0$), while downstream migration takes place in region III ($\omega > 0$).

This result can be given a simple physical explanation on the basis of the behaviour of the phase lags δ_1 and δ_2. The dependence of the angular frequency ω on such phase lags is readily written in the form:

$$\frac{\omega}{Q_0} = \frac{\lambda Q_{sr}}{\eta_r} \cos \delta_1 + \frac{m\pi Q_{nr}}{2\eta_r} \sin \delta_2. \qquad (7.3)$$

The direction of migration of linearly unstable alternate bars is then controlled by the balance between the two terms on the right-hand side of equation (7.3).

In figure 8, δ_1 and δ_2 are plotted versus bar wavenumber λ for two different values of β, corresponding to sub- and super-resonant conditions, respectively.

The second term of the right-hand side of (7.3) proves to be invariably positive, regardless of the values taken by β and λ, thus determining a contribution to bar
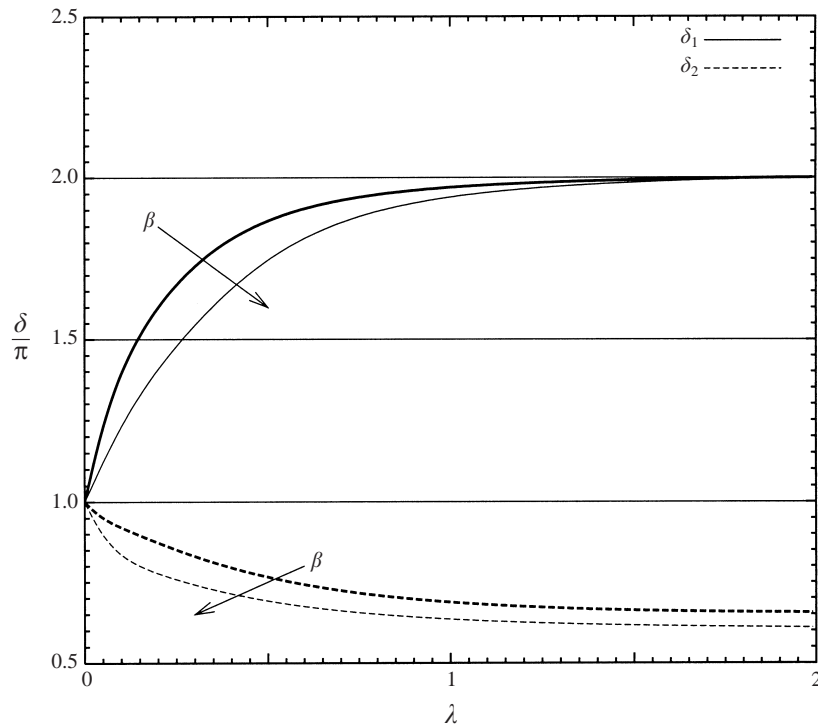
FIGURE 8. The phase lags δ_1 and δ_2 of the longitudinal and transverse components of the perturbed bedload vector (Q_{s1}, Q_{n1}) relative to bed topography are plotted versus bar wavenumber λ for $\beta = 10 < \beta_R$ and $\beta = 20 > \beta_R$ (plane bed, $\tau_* = 0.1$, $d_s = 0.01$, $\beta_R = 16.5$).

migration always in the downstream direction. On the contrary, the first term is negative for low values of λ, and becomes positive when λ exceeds a threshold value λ_* which increases with β. As a result, for sufficiently large values of the width ratio β, the first term on the right-hand side of (7.3) may prevail leading to upstream migration of the perturbations. The minimum value of β such that upstream migration may occur is the resonant value β_R and the corresponding wavenumber is the resonant wavenumber λ_R.

We may wonder why the phase lag of Q_{s1} changes quadrant (from the fourth to the third) for small values of the perturbation wavenumber λ, thus leading to upstream migration. In order to clarify this point, we note that perturbations of the longitudinal component of bedload flux are proportional to perturbations of the longitudinal component of bottom stress. As $\lambda \to 0$, longitudinal variations of all flow quantities tend to vanish, hence, flow continuity suggests that perturbations of the transverse component of velocity tend to vanish. Hence, the transverse component of the momentum equation implies that perturbations of free-surface elevation also tend to vanish, i.e. flow depth is in opposition relative to bottom elevation. The longitudinal component of the momentum equation, in the absence of inertial and gravitational effects, simply implies that perturbations of the ratio between longitudinal bottom stress and flow depth must vanish, hence, perturbations of the former must be in phase with perturbations of the latter. In other words, as $\lambda \to 0$, perturbations of bottom stress tend to have a phase lag π relative to bottom elevation, as shown by the complete solution plotted in figure 8.
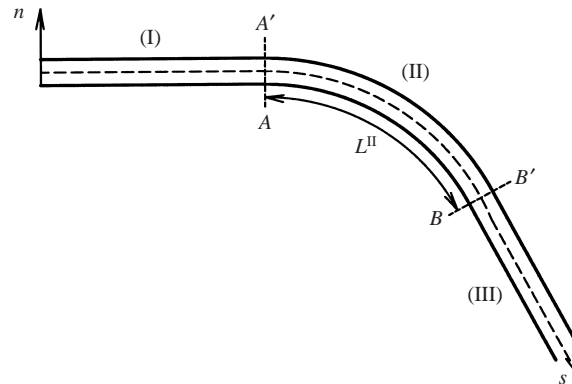
FIGURE 9. Overdeepening: sketch of the channel.

Finally, we point out that such an upstream migrating perturbation would not arise spontaneously, say in a straight channel, as, for given value of $\beta > \beta_R$, such perturbations are not the most unstable (see dashed line in figure 5). However, the development of such perturbations may be forced by geometrical constraints, such as the abrupt change in channel curvature leading to the phenomenon of overdeepening.

The above result was also implied in previous works (Johannesson & Parker 1989, Seminara & Tubino, 1992), but its relevance for the issue of morphodynamic influence does not seem to have been pointed out before.

8. An application to the overdeepening phenomenon and some discussion

In order to clarify the two scenarios described at the end of §6, let us employ the exact solution of the linear problem of meander morphodynamics to study the overdeepening phenomenon outlined in §1. We then focus our attention on an erodible channel consisting of a curved reach (II in figure 9) with constant curvature of the channel axis connected to two straight reaches located upstream (I) and downstream (III). Reaches (I) and (III) are assumed to be indefinitely long.

The exact solution of the linear model requires appropriate boundary conditions in order to evaluate the constants $c_{mj}(j = 1\text{–}4; m \geq 1)$. The curvature of channel axis exhibits discontinuities in the two cross-sections located at $s = 0$ and $s = s_L$. The solution is then obtained for the three reaches separately and matching conditions are imposed at the latter cross-sections. Having assumed reaches I and III to be infinitely long, the appropriate boundary conditions impose that perturbations of the flow and bottom topography must keep finite as $s \to \pm\infty$.

We now show that the phenomenon of overdeepening takes place downstream of cross-sections A–A′ and B–B′ provided the aspect ratio of the channel does not exceed the resonant value β_R. In fact, under such conditions, it turns out that:

$$\lambda_{m1} > 0 \ (m \geq 1), \qquad \lambda_{mj} < 0 \ (j = 2, 3, 4; m \geq 1). \tag{8.1}$$

Hence, each free mode m consists of four components, one of which is exponentially growing downstream, while the remaining three are exponentially decaying. Hence, the solution reads:

$$I - V_m = c_{m1}^I \boldsymbol{f}_{(1)} \exp(\lambda_{m1}s), \tag{8.2}$$
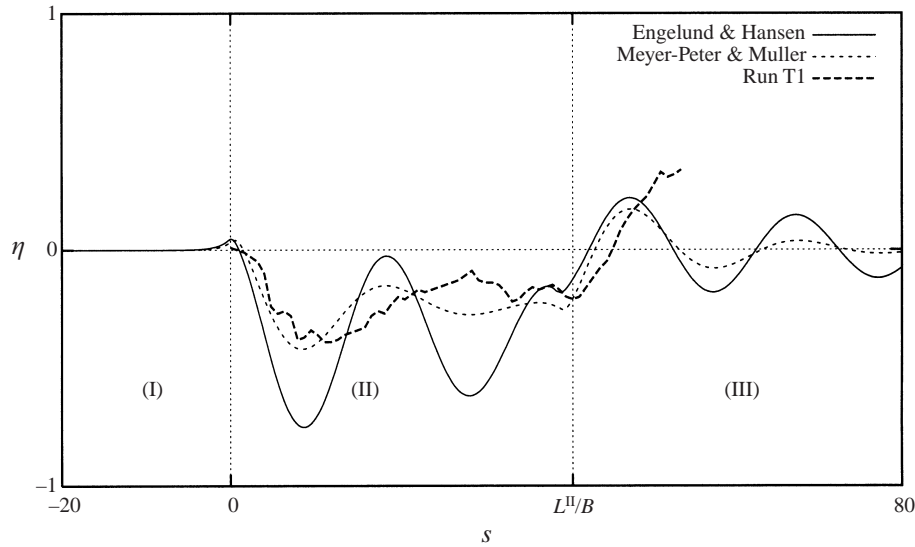
FIGURE 10. A comparison with run T1 of Struiksma *et al.* is performed by employing both Meyer–Peter & Muller's and Engelund & Hansen's formula.

$$II - V_m = c_{m1}^{II} \boldsymbol{f}_{(1)} \exp\left[\lambda_{m1}\left(s - \frac{L^{II}}{B}\right)\right]$$
$$+ \sum_{j=2}^{4} c_{mj}^{II} \boldsymbol{f}_{(j)} \exp\left(\lambda_{mj}s\right) + \hat{A}_m \sum_{j=1}^{4}\left[\frac{g_{j0}}{\lambda_{mj}}\boldsymbol{f}_{(j)} - \Gamma_{j1}^{(u,v,d,h)}\right], \qquad (8.3)$$

$$III - V_m = \sum_{j=2}^{4} c_{mj}^{III} \boldsymbol{f}_{(j)} \exp\left[\lambda_{mj}(s - L^{II}/B)\right], \qquad (8.4)$$

where the eight constants $c_{m1}^{I}, c_{mj}^{II}, (j = 1,\ldots,4), c_{mj}^{III}, (j = 2,\ldots,4)$ are readily calculated by imposing the matching conditions, $V_m = (u_m, v_m, d_m, h_m)$ and $\boldsymbol{f}_{(j)} = (1, \varphi_{mj}, \delta_{mj}, \xi_{mj})$, $j = 1,\ldots,4$. We have evaluated the solution for η ($= F_0^2 h - d$) by truncating the expansion (5.13) at the fifth order, as higher-order contributions decrease rapidly as m increases.

Good agreement is found with the experimental findings of Struiksma *et al.* (1985), referring to the sub-resonant case. The comparison is given in figures 10–12. Notice that the assumption of wide cross-sections employed in the present analysis, quite suitable to natural channels, is only approximately satisfied by the experimental conditions set up by Struiksma *et al.* In particular, the channel banks were vertical in the experiments, which implies that the effective width of the cross-section, practically unaffected by the presence of the sidewalls, was slightly smaller than the actual width of the channel. The relatively narrow character of the cross-sections was accounted for by applying our theory to effective cross-sections, treated as infinitely wide, and such that, under uniform flow conditions, they would carry the same discharge as the actual channel with a transversely uniform distribution of longitudinal velocity. The effective width of such a channel ($2B_e^*$) was related to the actual width ($2B^*$) by the following relationship

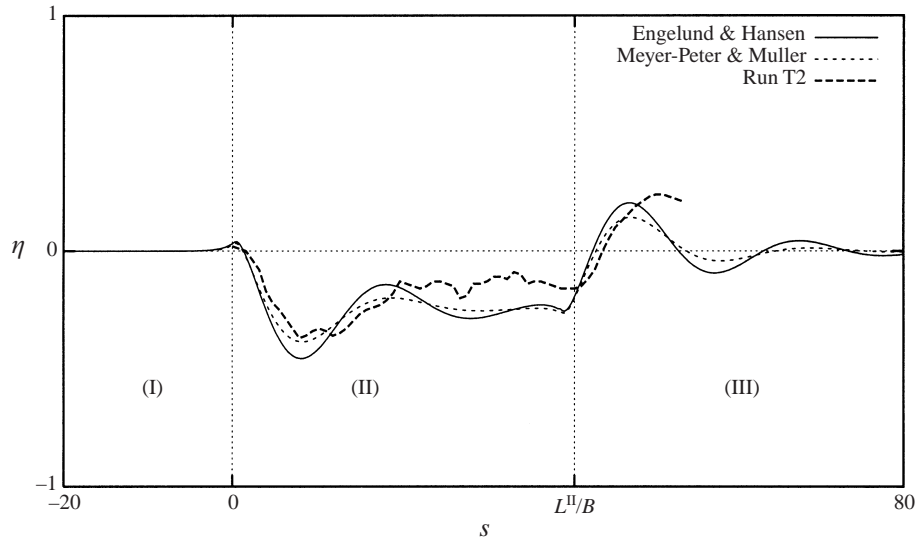$$\frac{B_e^*}{B^*} = \left(1 + \frac{D^*}{B^*}\right)^{2/3}. \qquad (8.5)$$

FIGURE 11. A comparison with run T2 of Struiksma *et al.* is performed by employing both
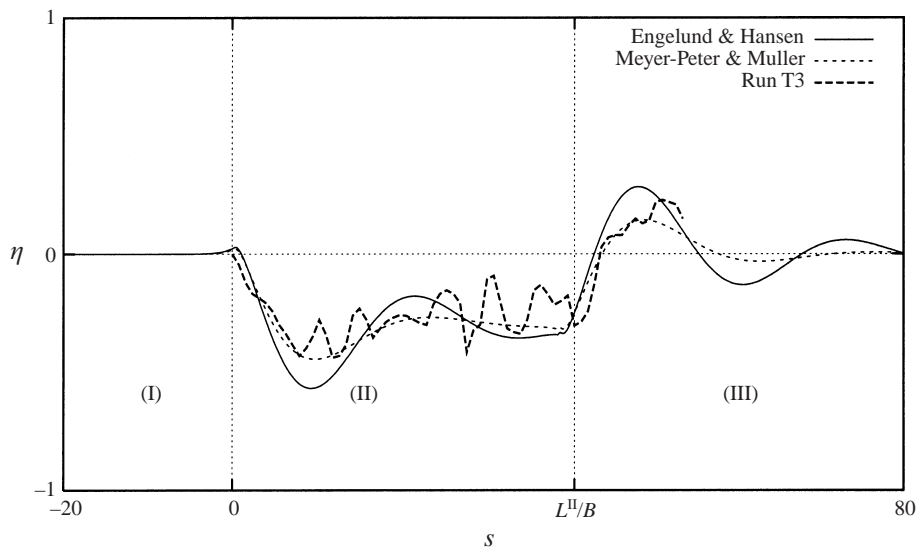Meyer-Peter & Muller's and Engelund & Hansen's formula.

FIGURE 12. A comparison with run T3 of Struiksma *et al.* is performed by employing both
Meyer-Peter & Muller's and Engelund & Hansen's formula.

Experimental conditions of run T1, T2, T3 of Struiksma *et al.* (1985) are reported in
table 1. The flume was 1.5 m wide and filled with almost uniform sand ($d_{50} = 0.45$ mm);
the bend was 29.32 m long, with $R_0^* = 12$ m.

Comparison is fairly satisfactory both for the wavelength and the amplitude of
bed deformations. Downstream overdeepening indeed occurs at the entrance of both
the curved reach (II) and of the straight reach (III), induced by the discontinuities
in channel curvature. Note that, in all examined cases, the value of the parameter
$v_0\sqrt{\tau_*}/rC_{f0}$ is lower than 10, hence, following Seminara & Solari (1998), we may
expect that the linear model is suitable for interpreting the actual phenomenon.

Run	Discharge $(m^3 s^{-1})$	Mean water depth (m)	Mean water velocity $(m s^{-1})$	Shields parameter
T1	0.047	0.080	0.39	0.26
T2	0.061	0.100	0.41	0.27
T3	0.074	0.091	0.54	0.52

TABLE 1. Experimental conditions of run T1, T2, T3 of Struiksma *et al.* (1985).

In fact, the agreement between the present theoretical results and the experimental observations of Struiksma *et al.* (1985) seems to be no less satisfactory than that achieved by Seminara & Solari (1998) on the basis of a two-dimensional nonlinear numerical model. However, note that no comparison has been performed with experiment T6 of Struiksma *et al.* (1985). The latter exhibited a fairly small value of β and its peculiar character was already noted by Struiksma *et al.* (1985). Furthermore, the present theory is unable to predict the occurrence of small-scale bottom perturbations exhibited by these experimental results. They are likely to arise from the nonlinear generation of higher-order longitudinal modes.

We then move to examine the occurrence of upstream overdeepening. In reach (I), the response of the system is characterized by three oscillating and exponentially growing free modes, whereas in reach (II) an exponentially damped free mode also contributes to the natural response. The complete solution is then obtained by adding the solution forced by curvature to the free response. In reach (III), only the exponentially damped free mode may contribute. In order to clearly isolate the upstream influence effect due to a discontinuity in channel curvature, the model is applied here to an even simpler channel configuration consisting of a straight reach (I) and a curved reach (II), supposed to be long enough for the effect of the downstream end not to be felt in the region of interest.

Figure 13 shows the bed profile close to the left bank of the channel, i.e. the outer bank of the bend. Notice that finite bed deformation occurs in the straight reach at a distance almost twenty times the channel width. In natural rivers, this would suggest a tendency of the upstream reach to undergo the process of bank erosion, leading to channel meandering. Experimental testing of this theoretical result is now being pursued in our laboratory. Preliminary results (Guala *et al.* 1999) support our theoretical findings.

It is then instructive to examine the exact solution (6.6) in relation to the standard model employed to simulate the planimetric evolution of meandering rivers. In fact, as already pointed out, nearly all available simulations are based on the linear morphodynamic model originally developed by Ikeda *et al.* (1981) and later modified by Johannesson & Parker (1989). The solution obtained by the standard model, written in the present notations is:

$$u_b = u|_{n=1} = \sum_{m=0}^{\infty} (-1)^m u_m$$

$$= v_0 \left[\mathscr{C}(s) + (\beta C_{f0})[A + F_0^2] \int_{s0}^{s} \exp[-2\beta C_{f0}(s-t)] \mathscr{C}(t) \, dt \right], \quad (8.6)$$

with A constant. Let us compare (6.6) with (8.6).

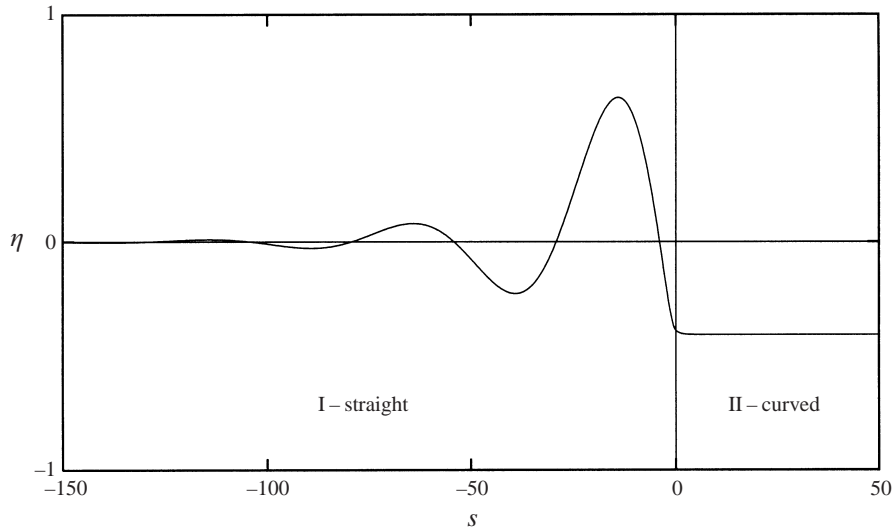The first significant difference arising from such comparison is that in (8.6) the non-

FIGURE 13. Upstream overdeepening: $\tau_* = 0.1$, $d_s = 0.01$, $\beta_R = 16.5$, $\beta = 30$.

history term involves only the value of local curvature, whereas the complete solution (6.6) also involves its derivatives up to some high order. As pointed out before, many of the additional terms included in (6.6) are quite small, being proportional to the dispersive coefficients k_2 and k_5, or to the higher derivatives of channel curvature. Other terms, namely those proportional to k_0, k_1, k_3 or k_4, appear in our linearized solution, though only terms proportional to k_3 play a dominant role. Their effect increases for the relatively short components of meander trains, which exhibit a fairly short life being intrinsically stable, as will appear in Part 2. However, on the whole, this feature does not seem to be too severe a limitation on the standard model.

A second, more significant, distinct feature of the complete model is its ability to account for upstream influence effects. In fact, some of the approximations on which the standard model is based make it only able to capture history effects which propagate downstream. Moreover, the kernel of the convolution integral in equation (8.6) is purely exponentially damped whereas the complete kernel is also oscillatory. Finally, the damping rate and the wavelength of oscillations in the complete formulation depend on β nonlinearly (see figure 4), rather than linearly as in (8.6). Such distinct features do have significant consequences on various aspects of river morphodynamics as will be shown in Part 2.

Finally, we point out that the restriction of linearity of the present model has a severe consequence in the super-resonant regime. In fact, Seminara & Tubino (1992) showed that exponentially growing modes tend asymptotically to reach a finite-equilibrium amplitude in the super-resonant regime. Hence, such modes, which cannot be included in linear theory, would arise in a nonlinear context, leading to a somewhat altered picture where upstream overdeepening would coexist with a downstream overdeepening, the latter being triggered by nonlinear growth in the downstream reach. A continuity for this effect will require the development of a fully nonlinear model.

The authors are grateful to G. Parker who kindly provided the data reported in figure 7.

Appendix A. Coefficients of equations (4.6)–(4.9)

$$f_{11} = -n\mathscr{C}\left(VU_{,n} + \beta\frac{\tau_s}{D}\right) - UV\mathscr{C} - n(k_0\Gamma_{n0} + k_1\Gamma_{n1} + k_2\Gamma_{n2}),$$

$$g_{11} = -k_0(\Gamma_0 + \Gamma_{s0}) - k_1(\Gamma_1 + \Gamma_{s1}) - k_2(\Gamma_2 + \Gamma_{s2}) + \mathscr{C}U^2 - n\mathscr{C}\left(VV_{,n} + H_{,n} + \beta\frac{\tau_n}{D}\right),$$

$$m_{11} = -\mathscr{C}(s)[n(DV)_{,n} + DV],$$

$$n_{11} = -\mathscr{C}(s)[Q_0(nq_{n,n} + q_n) + (F_0^2 H - D)_{,t}].$$

Coefficients $\Gamma_{n0}, \Gamma_{n1}, \Gamma_{n2}, \Gamma_{s0}, \Gamma_{s1}, \Gamma_{s2}$ and $\Gamma_0, \Gamma_1, \Gamma_2$ are defined as follows:

$$\Gamma_{n0} = \frac{\mathscr{C}}{\beta\sqrt{C_{f0}}}[U^2 D_{,n} + (DU^2)_{,n}],$$

$$\Gamma_{n1} = \frac{1}{\beta^2 C_{f0}}\{DU(U\mathscr{C})_{,s}D_{,n} + [D^2 U(U\mathscr{C})_{,s}]_{,n}\},$$

$$\Gamma_{n2} = \frac{\mathscr{C}}{\beta^2 C_{f0}}[U^2 D_{,s}D_{,n} + (DU^2 D_{,s})_{,n}],$$

$$\Gamma_{s0} = \frac{1}{\beta\sqrt{C_{f0}}}[\mathscr{C}U^2 D_{,s} + (\mathscr{C}U^2 D)_{,s}],$$

$$\Gamma_{s1} = \frac{1}{\beta^2 C_{f0}}\{DU(U\mathscr{C})_{,s}D_{,s} + [D^2 U(U\mathscr{C})_{,s}]_{,s}\},$$

$$\Gamma_{s2} = \frac{1}{\beta^2 C_{f0}}\{\mathscr{C}(UD_{,s})^2 + [\mathscr{C}DU^2 D_{,s}]_{,s}\},$$

$$\Gamma_0 = \frac{2\mathscr{C}}{\beta\sqrt{C_{f0}}}[UVD_{,n} + (UVD)_{,n}],$$

$$\Gamma_1 = \frac{2}{\beta^2 C_{f0}}\{DV(U\mathscr{C})_{,s}D_{,n} + [D^2 V(U\mathscr{C})_{,s}]_{,n}\},$$

$$\Gamma_2 = \frac{2\mathscr{C}}{\beta^2 C_{f0}}[UVD_{,s}D_{,n} + (DUVD_{,s})_{,n}].$$

REFERENCES

ANDREWS, E. D. 1984 Bed-material entrainment and hydraulic geometry of gravel-bed rivers in Colorado. *Geol. Soc. Am. Bull.* **95**, 371–378.

BECK, S. 1984 Mathematical modeling of meander interaction. In *River Meandering* (ed. C. M. Elliott), pp. 932–941. ASCE.

BECK, S., MELFI, D. A. & YALAMANCHILI, K. 1984 Lateral migration of the Genessee River, New York. In *River Meandering* (ed. C. M. Elliott), pp. 510–517. ASCE.

BLONDEAUX, P. & SEMINARA, G. 1985 A unified bar-bend theory of river meanders. *J. Fluid Mech.* **157**, 449–470.

CHIEN, N. 1954 The present status of research on sediment transport. *J. Hydraul. Div. ASCE*, **80**.

CODDINGTON, E. A. & LEVINSON, N. 1955 *Theory of Ordinary Differential Equations*. McGraw-Hill.

COLOMBINI, M., SEMINARA, G. & TUBINO, M. 1987 Finite-amplitude alternate bars. *J. Fluid Mech.* **181**, 213–232.

COLOMBINI, M., TUBINO, M. & WHITING, P. 1992 Topographic expression of bars in meandering channels. In *Dynamics of Gravel-Bed Rivers* (ed. P. Billi, R. D. Hey, C. R. Thorne & P. Tacconi), pp. 457–474. John Wiley.

CROSATO, A. 1990 Simulation of meandering river processes. *Commun. Hydraul.* Delft University of Technology, Rep. 3-90

DEAN, R. B. 1974 *Aero. Rep. 74-11*. Imperial College, London.

ENGELUND, F. & HANSEN, E. 1967 *A Monograph on Sediment Transport in Alluvial Streams*. Danish Technical Press, Copenhagen.

FURBISH, D. J. 1988 River-bed curvature and migration: how are they related? *Geology* **16**, 752–755.

GARCIA, M. & NINO, Y. 1993 Dynamics of sediment bars in straight and meandering channels: experiments on the resonance phenomenon. *J. Hydraul. Res.* **31**, 739–761.

GUALA, G., ZOLEZZI, G., BRANCA, A. & SEMINARA, G. 1999 Preliminary experimental observations of upstream overdeepening. *IAHR Symp. on River, Coastal and Estuarine Morphodynamics, Genoa, 6–10 September*.

HASEGAWA, K., NAKAMURA, K. & TOYABE, T. 1998 Analysis of experimental bed topography data with resonance conditions in meandering channels using linear theories. *J. Hydrosci. Hydraul. Engng* **16**, 73–86.

HOWARD, A. D. 1996 Modelling channel evolution and floodplain morphology. In *Floodplain Processes* (ed. M. G. Anderson, D. E. Walling & P. D. Bates). John Wiley.

IKEDA, S., PARKER, G. & SAWAI, K. 1981 Bend theory of river meanders. Part 1. Linear development. *J. Fluid Mech.* **112**, 363–377.

JOHANNESSON, J. & PARKER, G. 1989 Linear theory of river meanders. In *River Meandering* (ed. S. Ikeda & G. Parker). Washington DC, Water Res. Monograph 12, pp. 181–214. Am. Geoph. Union.

KALKWIJK, J. P. TH. & DE VRIEND, H. J. 1980 Computation of the flow in shallow river bends. *J. Hydraul. Res.* **18**, 327–342.

KELLERHALS, R., NEILL, C. R. & BRAY, D. I. 1972 Hydraulic and geomorphic characteristics of rivers in Alberta. *Alberta Cooperative Research Program in Highway and River Engineering, Edmonton, Alberta, Canada*.

KEVORKIAN, J. & COLE, J. D. 1981 *Perturbation Methods in Applied Mathematics*. Springer.

KINOSHITA, R. 1961 Investigation of channel deformation in Ishikari River. *Rep. Bureau of Resources, Dept Science and Technology, Japan*.

KOVACS, A. & PARKER, G. 1994 A new vectorial bedload formulation and its application to the time evolution of straight river channels. *J. Fluid Mech.* **267**, 153–183.

LANGBEIN, W. B. & LEOPOLD, L. B. 1964 Quasi equilibrium states in channel morphology. *Am. J. Sci.* **262**, 782–794.

MACDONALD, T. E., PARKER, G. & LEUTHE, D. P. 1991 Inventory and analysis of stream meander problems in Minnesota. *Res. Rep. St Anthony Falls Hydraulic Laboratory, University of Minnesota*.

ODGAARD, A. J. 1986 Meander flow model. I: development *J. Hydraul. Engng ASCE* **112**, 1117–1136.

OLESEN, K. W. 1983 Alternate bars and meandering of alluvial rivers. *Commun. Hydraul. Delft University of Technology Rep.* 7–83.

PARKER, G. 1990 Surface-based bedload transport relation for gravel rivers. *J. Hydraul. Res.* **20**, 417–436.

PARKER, G. & ANDREWS, E. D. 1986 On the time development of meanders bends. *J. Fluid Mech.* **162**, 139–156.

PARKER G., DIPLAS, P. & AKIYAMA, J. 1983 Meanders bends of high amplitude. *J. Hydraul. Engng ASCE* **109**, 1323–1337.

ROZOVSKIJ, I. L. 1957 *Flow of Water in Bends of Open Channel*. Acad. Sci. Ukrainian SSR, Kiev.

SEMINARA, G. & SOLARI, L. 1998 Finite amplitude bed deformations in totally and partially transporting wide channel bends. *Water Resour. Res.* **34**, 1585–1594.

SEMINARA, G. & TUBINO, M. 1992 Weakly nonlinear theory of regular meanders. *J. Fluid Mech.* **244**, 257–288.

SEMINARA, G., ZOLEZZI, G., TUBINO, M. & ZARDI, D. 2001 Downstream and upstream influence in river meandering. Part 2. Planimetric development. *J. Fluid Mech.* **438**, 213–230.

SEKINE M. & PARKER, G. 1992 Bed load transport on transverse slope – I. *J. Hydraul. Engng ASCE*, **118**, 513–535.

SHIMIZU, Y., TUBINO, M. & WATANABE, Y. 1992 Numerical calculations of bed deformation in a range of resonant wavenumbers in meandering channels. *Proc. Hydraul. Engng JSCE*, **36**, 15–22.

STOLUM, H. 1996 River meandering as a self-organization process. *Science* **271**, 1710–1713.

STRUIKSMA, N., OLESEN, K. W., FLOKSTRA, C. & DE VRIEND, H. J. 1985 Bed deformation in curved alluvial channels. *J. Hydraul. Res.* **23**, 57–79.

SUN, T., MEAKING, P., JOSSANG, T. & SCHWARZ, K. 1996 A simulation model for meandering rivers. *Water Resour. Res.* **32**, 2937–2954.

TALMON, A. M., STRUIKSMA, N. & VAN MIERLO, M. C. L. M. 1995 Laboratory measurements of the direction of sediment transport on transverse alluvial-bed slopes. *J. Hydraul. Res.* **33**, 519–534.

TUBINO, M. & SEMINARA, G. 1990 Free-forced interactions in developing meanders and suppression of free bars. *J. Fluid Mech.* **214**, 131–159.

VRIES, M. DE 1969 Riverbed variations. Aggradation and degradation. *IAHR Seminar, New Delhi.*

WHITING, P. J. & DIETRICH, W. E. 1993 Experimental studies of bed topography and flow patterns in large-amplitude meanders. 1. Observations. *Water Resour. Res.* **29**, 3605–3622.